



Laser photothermal non-destructive inspection method for hairline crack detection in unsintered automotive parts: A statistical approach

Jordan Tolev*, Andreas Mandelis

Center for Advanced Diffusion–Wave Technologies, Department of Mechanical and Industrial Engineering, University of Toronto, Toronto, ON, Canada M5S 3G8

ARTICLE INFO

Article history:

Received 26 June 2009

Received in revised form

1 February 2010

Accepted 15 February 2010

Available online 6 March 2010

Keywords:

Non-destructive inspection

Photothermal radiometry

Crack detection

ABSTRACT

A statistical non-contacting and non-intrusive method for revealing the presence of cracks in unsintered (green) parts manufactured by powder metallurgy (PM) technology was developed based on photothermal radiometry (PTR). The technique relies on the interaction of a modulated laser-generated thermal wave with the crack resulting in change of amplitude and phase of the detected signal. The crack existence at points in high stress regions of a group of green sprockets was evaluated through the proposed method. The results were validated by an independent destructive technique—microscope observation of the tested green sprockets following sintering, sectioning, and polishing at the locations where signal changes were observed in the green state. Statistical analysis confirmed the excellent sensitivity (91%) of the method in detecting the presence of hairline ($\sim 5\text{--}10\ \mu\text{m}$) cracks. This PTR diagnostic technique may lead to a simple and reliable on-line inspection methodology in high-stress locations of PM manufactured industrial steel products. Ultimately, the method can be developed for non-destructive quality and feedback control of the metal forming process of green automotive parts.

© 2010 Elsevier Ltd. All rights reserved.

1. Introduction

The manufacture of steel components produced from powder metallurgy technologies with high precision and low production cost has steadily increased in recent years. Automotive components such as sprockets, clutch plates, and other parts usually operate under high strain. In view of their critical functionality, there exist stringent quality and reliability requirements. Two most significant defect types in powder metallurgy parts are surface and subsurface micro-cracks near regions of high stress concentration such as at corners and steps. These micro-cracks can appear during the forming process in the green (unsintered) state; they remain after sintering and may cause serious, even catastrophic, damage. The powder metallurgy industry's Vision and Technology Roadmap [www.mpif.org, 2001] has identified as a critical barrier of enabling technologies the inability to measure internal cracks in unsintered parts.

Nowadays, industry uses various non-destructive testing methods such as Eddy current, acoustic, magnetic, resistivity, and X-ray detection techniques [1] for diagnosing defective elements not in the green state, but only after sintering. Currently, with the dramatic increases in global energy prices it is ill afforded and

expensive for the automotive parts manufacturing industry to dispose of, and effectively waste, defective sintered components. A highly desirable solution of this problem would be the detection of the presence of cracks in automotive parts in the green state. Then, the identified defective parts can be easily reduced to metal powder, which can be recycled toward the manufacture of new components. However, to the best of our knowledge, until now there exists no non-destructive testing technique capable of detecting of cracks in the green manufactured state, especially at the early nucleation stage (micron size or hairline).

In the past 25 years several photothermal techniques have been proposed for monitoring subsurface crack in solids, [2], including a microphone-cell photoacoustic setup [3], a laser pump-probe photothermal displacement method (Mirage effect) [4], and a photopyroelectric needle probe method [5]. Theoretical and experimental studies [6–9] have been performed with the goal to apply infrared techniques for testing crack presence in green-state PM parts. These techniques involve static (dc) imaging using a mid-IR camera and based on detection of the thermal radiation emitted as a result of the industrial process of part forming (passive heat response) [6] or produced after direct electrical current heating or electromagnetic coil-induced eddy current generation (active heat response) [7–9]. Unlike modulated thermal-wave and other techniques such as induction heating, with static imaging methods using the passive heat response of the part forming process it would be difficult or impossible to

* Corresponding author.

E-mail address: tolev@mie.utoronto.ca (J. Tolev).

identify spatially confined hairline cracks as they often appear in manufactured automotive parts due to the absence of a light-modulation-frequency-controlled characteristic (e.g. thermal diffusion) length which can be adjusted to match the size of the crack. However, research to-date [6–9] has shown that it is possible to discern variations in the thermal profiles of sequentially manufactured parts that could be indicative of defects generated during the manufacturing process. Following external heating, the presence of a crack perturbs the local temperature field, which is recorded with the camera and shown in the IR image. These images are compared with a reference image of an intact sample [9] and the existence of μm -size cracks becomes evident. Nevertheless, these techniques have addressed relatively smooth sample geometries at easy-to-reach locations and the detected cracks have been artificially created on a flat surface. There has been no reported thermal technique involving a combination of real manufacturing-induced sub-surface cracks and complex part geometries such as internally recessed corners or abrupt surface slope changes (steps).

Existing methods for non-destructive testing can be broadly classified in the following categories: X-ray radiographic techniques, acoustic (ultrasonic, US) methods, electrical resistivity inspection, and visual inspection including pressure testing. X-ray techniques can detect cracks in green powder metallurgy parts but they are ionizing radiation and the detection of cracks depends on their orientation relative to the direction of the propagation of the X-ray field. Ultrasound can monitor defects in solids. US waves are reflected from interfaces in a sample, including cracks as well as free surfaces. The characterization of the green state by US methods, however, appears to be hindered by the problem of extreme attenuation of the incident signal. The velocity of US waves in green compacted samples is about half the velocity in sintered compacts and essentially invariant with density [10]. Furthermore, the velocity of ultrasound in green parts is highly anisotropic and experimental reproducibility is very poor. In addition, the requirement for bath immersion in order to overcome the air impedance to US propagation and produce a high-SNR signal is an issue impacting the applicability of this method for high throughput on-line implementation in industrial settings. Several techniques exist for electrical resistivity testing. One is a direct impedance testing. An applied potential sets up an electric field within a conductive solid, which creates currents influenced by structural irregularities, including cracks and porosity. Green compacted samples, however, are poor electrical conductors, their resistivity being an order of magnitude higher than that of their sintered counterparts. Therefore, they are much less sensitive to resistivity perturbations by defects (cracks and porosity). Besides, there are two additional potential contributors to the non-reliability of the resistivity test. First, in addition to cracks, edges, and corners distort the current fields; it is important to note that machined high-stress internal corners of parts are often the sites of green cracks. Next, when the oxide layer on green-part particle cluster surfaces is altered with thermal treatments, the resistivity of the green parts decreases [10]. An important non-contact form of resistivity testing is eddy currents. The AC current in the induction coil can vary from 1 to 1000 kHz. Penetration depth varies with frequency, with the highest frequencies yielding the smallest depths (skin effect). As mentioned above, this method is quite similar to thermal waves in its detection mechanism. Disruptions in the eddy current path due to any defect (for example crack) that changes the resistivity of the material are detected as extraneous induced voltages in the induction coil. A disadvantage of this method is the small penetration depth of the eddy current and the influence of the complicated form of the parts [2]. Visual inspection and pressure testing include magnetic particle inspection test and liquid dye

penetration inspection. These NDT techniques are essentially lab methods and are impossible to use for crack detection in green parts because they cannot differentiate between the porosity of pressed powder green materials and the presence of hair-size flaws. These test techniques can detect cracks in green compacts but they are truly lab methods and it is impossible to use them for line crack detection in industrial conditions. At present none of the abovementioned test techniques is used in industry with green parts and crack testing procedures are applied only after the sintering of parts. In the text we have now inserted an abbreviated version of the foregoing discussion.

Therefore, motivated by the potential of PTR for non-destructive testing and keen industrial demand for quality control in volume production of a variety of powder metallurgy manufactured automotive parts with complicated shapes, we undertook a study of subsurface crack detection using laser-induced thermal waves and industrial powder metallurgy parts in the green state. The presence of a crack changes the amplitude and phase of the detected signal, which is blackbody (Planck) radiation emitted by the sample upon optical heating with an intensity-modulated laser beam, following conduction of the thermal wave to the region of the crack and thermal interaction with it. It is well known that thermal-wave propagation is sensitive to material discontinuities in the form of delaminations, which is what the air gap (crack) effectively is, when the distance of the discontinuity from the thermal-wave source (surface) is on the order of one thermal wavelength. Although the thermal wavelength may be large compared to crack thickness, the field is very sensitive to interface properties such as the thermal reflection (more properly accumulation or depletion) coefficient, especially when the properties of the two sides of the interface (powder material and air gap in the case of a crack) are very different. This property allows for sensitivity of the thermal-wave signal to hairline crack discontinuities, despite the large size of the thermal wavelength compared to crack thickness. Signal changes depend on the difference between the thermal parameters of the green powder material and those of the crack, the position, and the geometry of the crack. In these situations, the crack acts as a thermal impedance to the propagation of the laser-induced thermal wave.

Clearly, a direct micro-crack diagnostic methodology for green-state manufactured automotive parts is of great importance to industrial quality control. In this work we demonstrate that this goal can be attained using dynamic thermal-wave propagation fields and their interactions with subsurface hairline cracks.

2. Experimental setup and methodology

An outline of the experimental system is shown in Fig. 1. A modulated heating laser beam (the second harmonic of a 1064 nm Nd:YAG laser; a green emission line at 532 nm) was focused on the surface of the inspected sample using a gradient lens and a micro-mirror. The laser beam size spot on the sample surface was 20 μm . The thus generated thermal infrared radiation was directed to an infrared mercury-cadmium-telluride (MCT) photodetector through two reflecting objectives. There the radiative flux is transformed to an electrical signal that is processed by a lock-in amplifier and a computer. The signal consists of the amplitude and phase of the thermal wave as a function of laser-intensity-modulation frequency at a fixed location on the sample or as a function of location during a line scan at a fixed frequency. Typically, low frequencies correspond to long pathlengths in the interrogated material ($\sim\text{mm}$) while high frequencies probe shorter distances ($\sim\mu\text{m}$), commensurate with the size of the monitored cracks. With this technique the “spatial resolution” of crack presence amounts to crack detection “threshold” that depends mostly on the relative position between

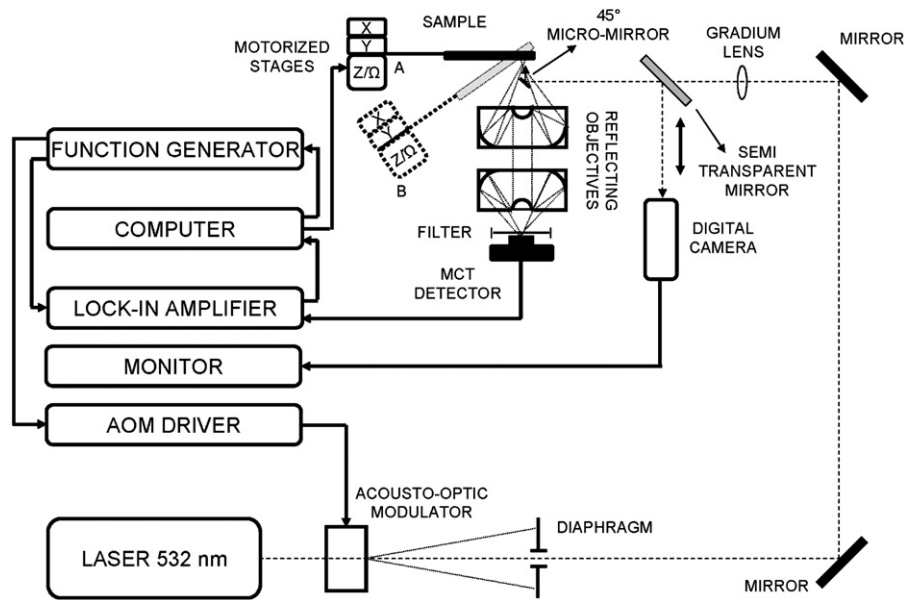


Fig. 1. Schematic of the experimental system for photothermal radiometry of subsurface hairline manufacturing cracks.

the diffusing thermal wave from a focused laser beam and the orientation of the crack. Positioning the circular sprocket samples for line scans outward from the center and frequency scans at specific polar angular directions was performed with the aid of motorized sample holder stages with linear and circumferential degrees of freedom. The system has the ability to scan the surface of an inspected sprocket circumferentially and radially at any angle θ between 45° and 135° (Fig. 1 positions A and B). The current angular limitations are imposed by the size and shape of the sprockets. Furthermore, the system has the ability to monitor the location of the laser spot through a digital camera and a semi-transparent mobile mirror (a microscope slide). Because of the semi-transparent mirror, the image from the camera was not very clear and was only used for rough adjustment of the position of the laser beam spot relative to the inner step of the sprockets (Fig. 2). That same semi-transparent mirror made it impossible to perform line scans and simultaneously monitor the position of the laser spot on the sample surface.

Exploratory line scans at fixed frequency were performed on the inner step of automotive transmission sprockets, shown on the drawing of Fig. 2. They encompassed parallel scans (circumferential trace along the step) and perpendicular scans (radial trace across the step). In the first phase of the project a large volume of experimental data (not shown in this paper) was obtained from circumferential line scans along the step. The data analysis showed that it is not possible to correlate the presence or absence of hairline cracks ($\sim 5\text{--}20\ \mu\text{m}$) along the circumference and the behavior of the amplitude and phase of the PTR signals. It was noted that the signals strongly depend on the constancy (or absence thereof) of the laser beam distance from the step on scan-related focal plane movements (beam defocusing), as well as on roughness and cleanliness of the surface. Among these strong signal-affecting factors, the influence of the cracks was negligible, especially if their size was less than $10\ \mu\text{m}$. Therefore, in order to optimize the crack contribution in the PTR signal generation, short radial scans were performed across (perpendicular to) the inner step, accompanied by frequency scans at locations in the immediate vicinity of the crack. Unfortunately, visual verification of the exact position of the laser beam was largely impeded, as explained above. It was found, however, that the PTR amplitude

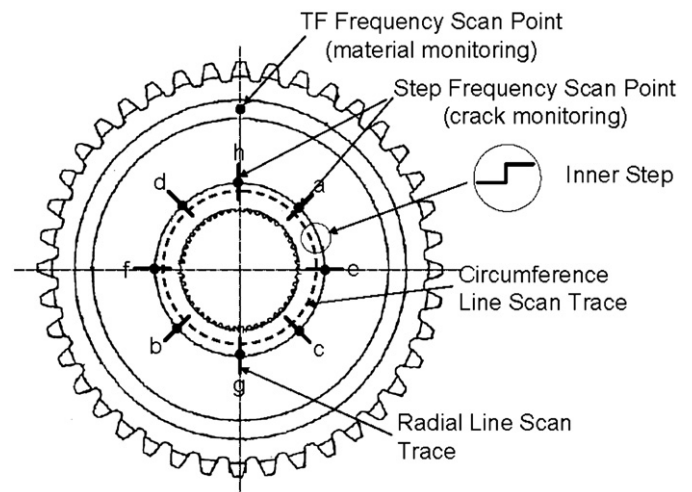


Fig. 2. Schematic drawing of circumferential and radial line scan and frequency scan locations on unsintered automotive transmission sprocket samples.

trace across the inner step provided a more accurate localization criterion than visual inspection using a CCD camera. The actual laser beam position was determined from the line scan trace of the PTR signal, such as the maximum and the onset of signal increase as the beam reached the step. The use of multiple frequencies allows probing of the PTR signal at various subsurface depths and optimizes the probability that the generated thermal waves will interact with neighboring subsurface cracks as the thermal diffusion length shrinks with increasing frequency. The thermal wavelength is proportional to the thermal diffusion length in the overlying solid layer, $\mu(f) = \sqrt{\alpha_s/\pi f}$, where α_s is the thermal diffusivity of the layer and f is the modulation frequency. Furthermore, the laser beam that generated the thermal wave was directed at a 45° angle to the sample surface in the vicinity of the step instead of the 90° normal, in expectation of symmetric positional flexibility along both sides of the vertical step walls and possibly stronger interaction with, and higher detectivity of, incipient cracks in the vicinity, as each crack was interrogated from both vertical walls.

3. Sample preparation and experimental results

A group of five green sprockets including “good” samples with very few or no subsurface cracks and “bad” samples with known extensive subsurface cracks near, or at, the inner step were delivered by an automotive parts manufacturer and were machined to reduce the thickness of the outer wall so as to make it easier to perform laser scans with short working distance optics (a reflective objective), which might otherwise interfere with the walls. The inner part of the sprockets, including the < 1 mm high step shown in Fig. 2, remained intact during the machining process. Two of the samples were without cracks (samples labeled “1” and “2”) and three with high probability of subsurface crack presence directly below, or in the immediate vicinity of, the inner step (samples labeled “3”, “4”, and “5”). The locations of the frequency scans were specified with radial line scans performed at eight radial directions (a, b, ..., h) in all samples, Fig. 2. After the PTR

measurements, these samples were sent back to the manufacturer for sintering and cutting 1-cm-wide cross-sectional slices, which included the eight radial spots (a, b, ..., h) scanned with PTR. The slices were further polished on both sectioned (side) surfaces, were placed on a microscope and microscope pictures were taken of the crack on both sides. In Fig. 3 we present cross-sectional microscope pictures of the two opposite side surfaces (sides 1 and 2) of the slices cut out of sprocket #3 after sintering at the eight radial directions (a, b, ..., h) with frequency scans performed in the green state at two specific spots defined through radial line scans at fixed frequency along each of these directions (see Fig. 2). The first spot (labeled “point v”) was at the foot of the signal amplitude peak due to the presence of the step. This location is not defined precisely. The second spot (labeled “point p”) was precisely at the peak amplitude position of the same trace. The mean values and standard deviations of amplitudes and phases for every frequency scan at the eight directions (a, b, ..., h) on the

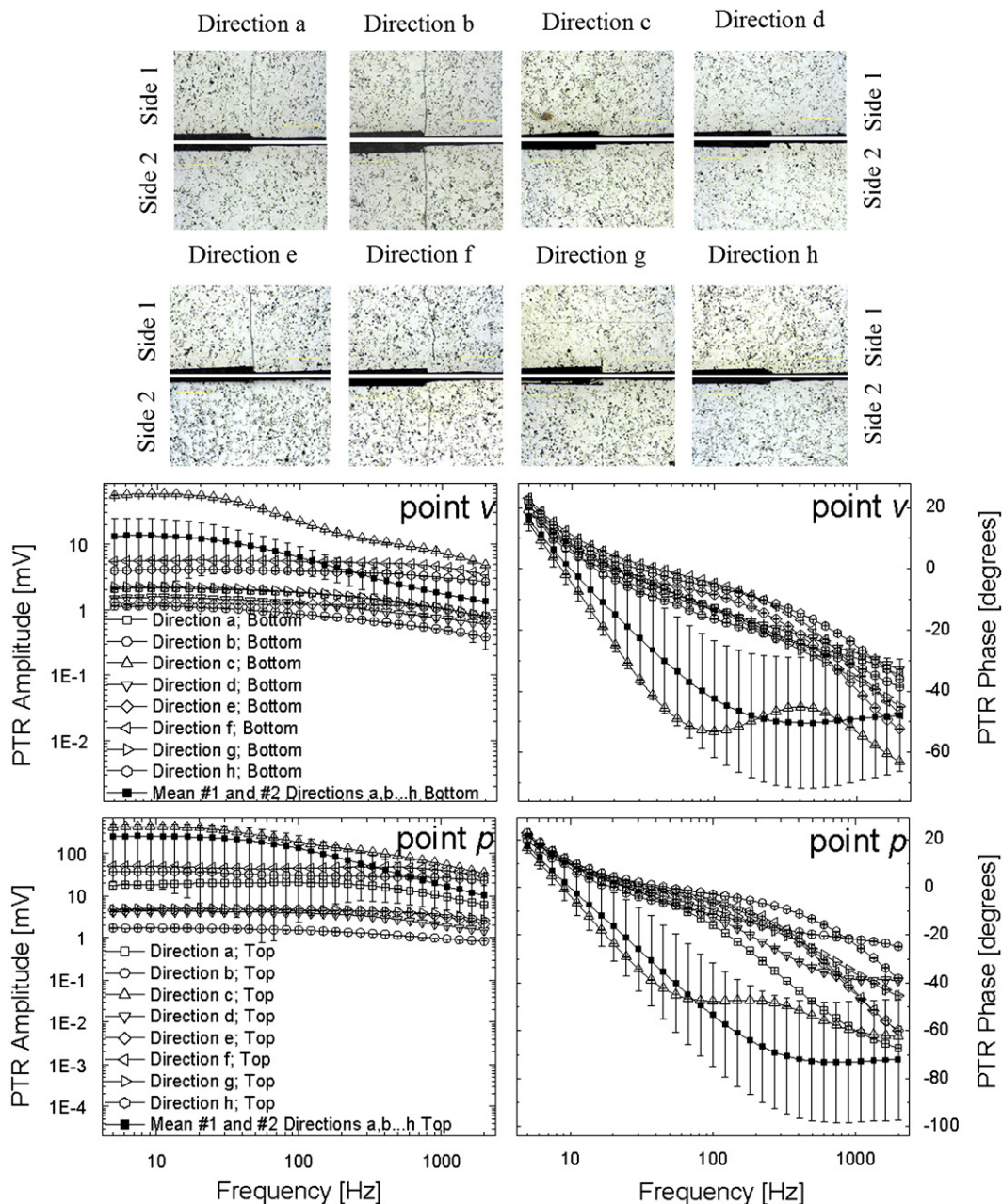


Fig. 3. Cross-sectional microscope pictures of sintered sprocket #3 at directions a, b, ..., h and frequency scans in the green state.

“good” samples (16 points in all) were used to generate reference amplitude and phase calibration frequency bands corresponding to non-cracked green samples at each of the two points p and ν . Similar pictures and graphs, not presented in this paper, were made for each one of the sprockets #1–5.

In Figs. 4 and 5 and we present plots of amplitudes and phases of frequency scans and line scans performed at direction \mathbf{b} on sample 4 and direction \mathbf{f} on sample 5, respectively, as well as the corresponding cross-sectional microscope pictures. In Figs. 6 and 7 and we present similar information from directions \mathbf{g} and \mathbf{b} on samples 1 and 2, respectively. It is obvious that the frequency-scan amplitudes have a strong dependence on sample surface irregularities and cannot be used for subsurface crack detection, as the inter-curve variance is larger than that caused by the presence of cracks. Nevertheless, the frequency scan phase graphs presented in Figs. 4 and 5 and at both probe points p and ν lie outside and above the corresponding non-cracked reference bands along significant portions, or the entirety of, the frequency spectrum 5–2000 Hz. The corresponding cross-sectional microscope photos of the side surfaces clearly show the presence of cracks under the steps. The crack in Fig. 4 has propagated through to the surface at, or above, the base of the step, whereas the crack in Fig. 5 has reached the surface (top photo) on one side, becoming a subsurface crack before it reached the other cross-sectional plane (bottom photo). It turns out that all cracks observed in the full complement of our sprocket samples belong to one or the other of these two categories and similar phase behavior was observed in the great majority of frequency scans (see Section 5). The observed phase lead of the cracked samples in Figs. 4 and 5 and compared to the reference band is understandable in terms of the confinement of the thermal wave within the region above the subsurface sheet crack/delamination, assuming air or quasi-vacuum as the inter-crack space filler acting like a thermal impedance. This confinement shifts the centroid of the thermal wave closer to the surface than in non-cracked samples, which amounts to a phase lead. The fact that the phase in Fig. 5 dives inside the non-cracked band above ca. 800 Hz at location point ν may, or may not, be the result of the thermal wavelength shrinking to distances shorter than the extent of the crest of the subsurface crack, thus losing sensitivity to it and behaving like a non-cracked sample. It is also possible that surface roughness dominates that high end of the frequency spectrum for both non-cracked and cracked samples. Conversely, as an example of non-cracked behavior, the frequency-scan phase graphs presented in Figs. 6 and 7 and, both points p and ν , are contained within the non-cracked reference bands.

Nevertheless, the small size of the cracks, but most importantly uncertainties in crack-laser beam relative positioning (which requires a tighter control of the scanning system than we currently possess) has led to exceptions from the aforementioned detection rules in the form of a few false positives and false negatives. In Figs. 8 and 9 and we demonstrate some such exceptions. Fig. 8 shows results from direction \mathbf{d} on sample 3 and Fig. 9 shows the same information from direction \mathbf{e} on sample 4. The phase frequency scan in Fig. 9 below ~ 40 Hz lies within the reference band, as expected from the bulk contributions to the thermal-wave signal of a sample in which the thermal wavelength is much longer than the crack size. However, despite the obvious crack beneath the step, the phase remains within this band throughout the frequency scan thus exhibiting a false negative behavior. On the other hand, the phase frequency scan in Fig. 8 above ~ 30 – 40 Hz rises almost entirely outside the reference band despite the absence of a crack as shown in the photos, thus exhibiting a false positive behavior. These anomalies are shaping PTR crack detection technology as a statistical analytical inspection technique, not unlike a number of other statistical NDT

methods dealing with natural or manufactured materials of variable geometries, texture, and densities.

Additional groups of frequency scans were made at points marked \mathbf{TF} located on the flat part of the surface of all samples (Fig. 2). According to the manufacturer at those points, the expectation of crack presence was null. Graphs of amplitude and phase frequency scans are presented in Fig. 10. The natural variance of phase from sample to sample in the two known uncracked (reference) sprockets 1 and 2 is very narrow and the remaining phase curves from the otherwise cracked sprockets tend to closely align with these two reference sample up to ~ 300 Hz, above which surface effects possibly dominate the signals. There is some divergence of the behavior of sample 4 above 30 Hz which may be attributed to excessive surface roughness outside the norm, as is also shown in the amplitude scan, Fig. 10a. From these results, additional support is garnered for the phase frequency scan as a sensitive measure of the presence or absence of subsurface cracks in green automotive sprockets.

4. Statistical analysis of the PTR data

Large amounts of data similar to Fig. 3, obtained along the radial directions \mathbf{a} , \mathbf{b} , ..., \mathbf{h} , Fig. 2, at points ν and p , respectively, on all five sprockets were subjected to statistical analysis to calculate the sensitivity and specificity of PTR as a detection technique of hairline subsurface cracks. The presence or absence of a crack in sliced sprockets placed under the microscope, and the resulting cross-sectional surface photos (both sides) taken at all radial directions shown in Fig. 2 were chosen as the golden standard in generating the non-cracked reference band statistics and validating the PTR phase frequency scans from cracked samples and their relative shifts outside the reference band. All phase frequency scan data were divided into four categories

1. *true positive*—at least one of the two-side photos shows a crack is present and the phase frequency scan also shows the crack presence by lying outside the reference band;
2. *true negative*—the photos show no crack is present and the phase frequency scan also shows the absence of a crack by entirely lying inside the reference band;
3. *false positive*—the photos show no crack is present, but the phase frequency scan shows a crack is present by lying outside the reference band;
4. *false negative*—at least one of the two-side photos shows a crack is present, but the phase frequency scan shows the absence of a crack by entirely lying inside the reference band.

The results from a generalized statistical analysis of the experimental PTR phase frequency scan data from the green sprocket 3 vs. the validation golden standard (cross-sectional photos of the sintered and subsequently sectioned sprocket #3, Fig. 3) are presented in Table 1. Similar tables, not presented in this paper, were made for each of the sprockets #1–5 and the results are summarized in Table 2. The sensitivity, specificity, and accuracy calculations of Table 2 were performed using the statistically accepted formulas:

$$\text{Sensitivity} = \text{true positive} / \text{actual positive instances};$$

$$\text{Specificity} = \text{true negative} / \text{actual negative instances};$$

$$\text{Accuracy} = (\text{true positive} + \text{true negative}) / (\text{actual positive instances} + \text{actual negative instances});$$

$$\text{Actual positive instances} = \text{true positive} + \text{false negative};$$

$$\text{Actual negative instances} = \text{true negative} + \text{false positive}.$$

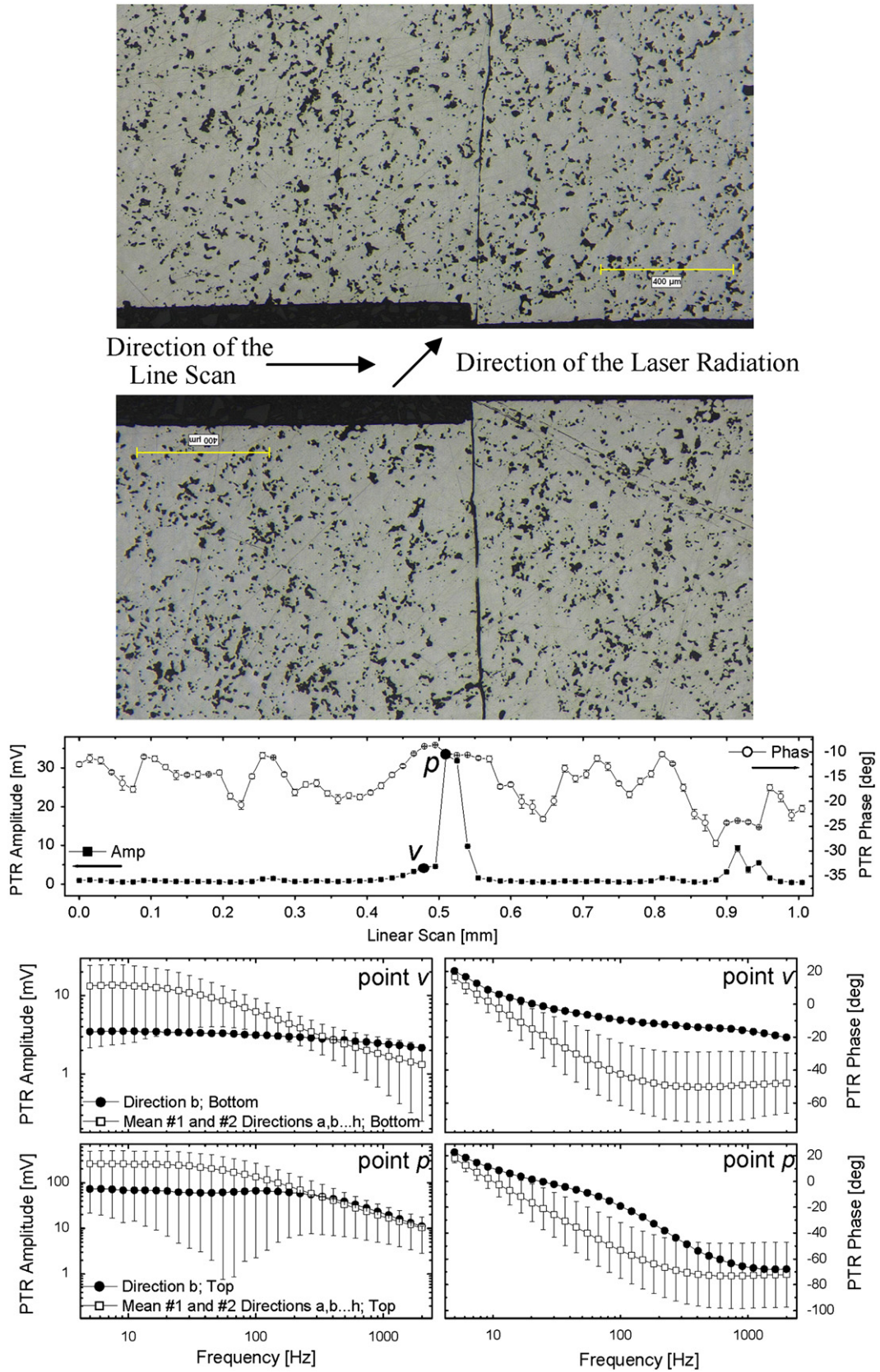


Fig. 4. Cross-sectional microscope pictures, radial line scan and frequency scans of green sprocket #4 at direction b.

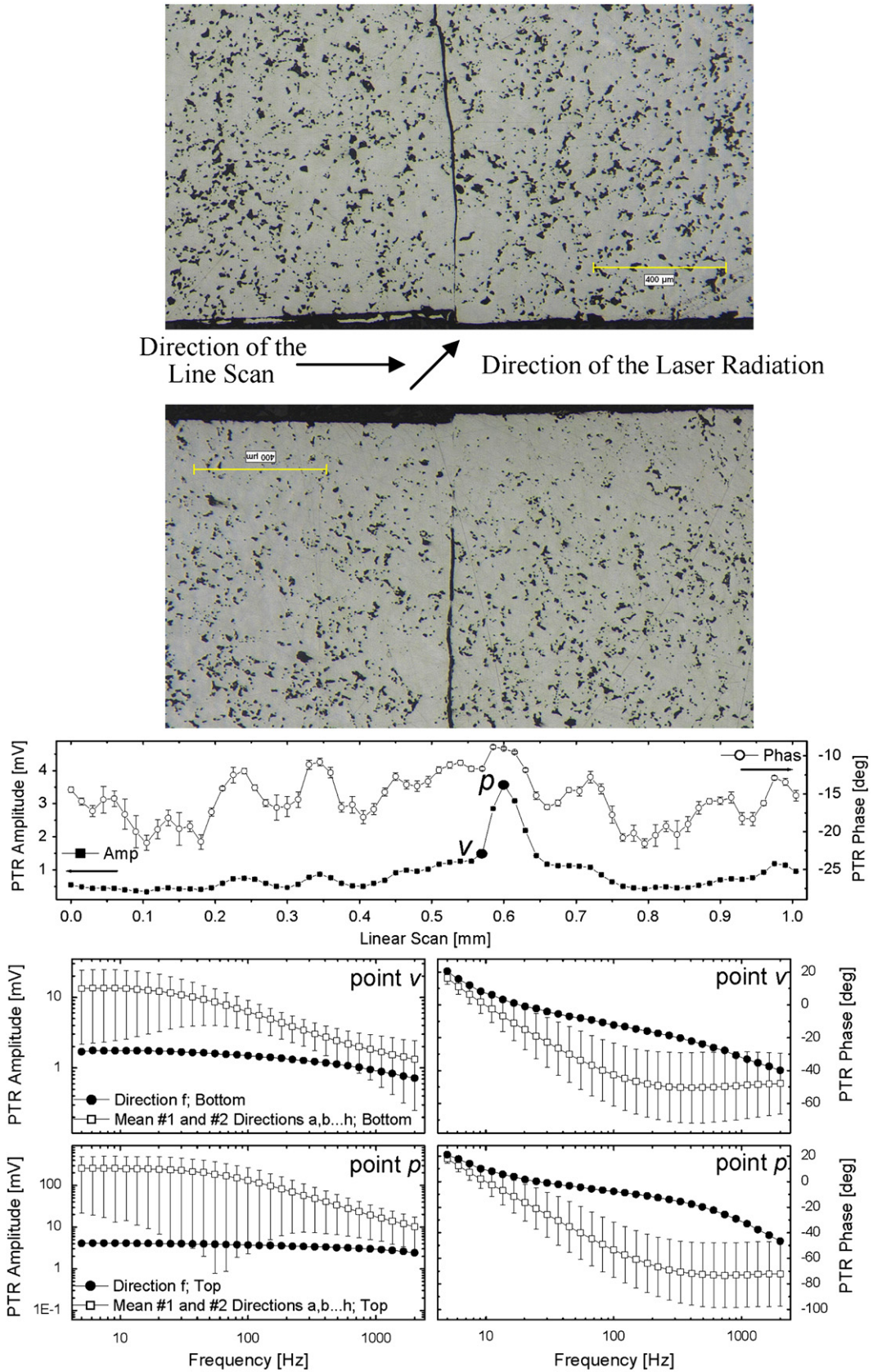


Fig. 5. Cross-sectional microscope pictures, radial line scan and frequency scans of green sprocket #5 at direction f.

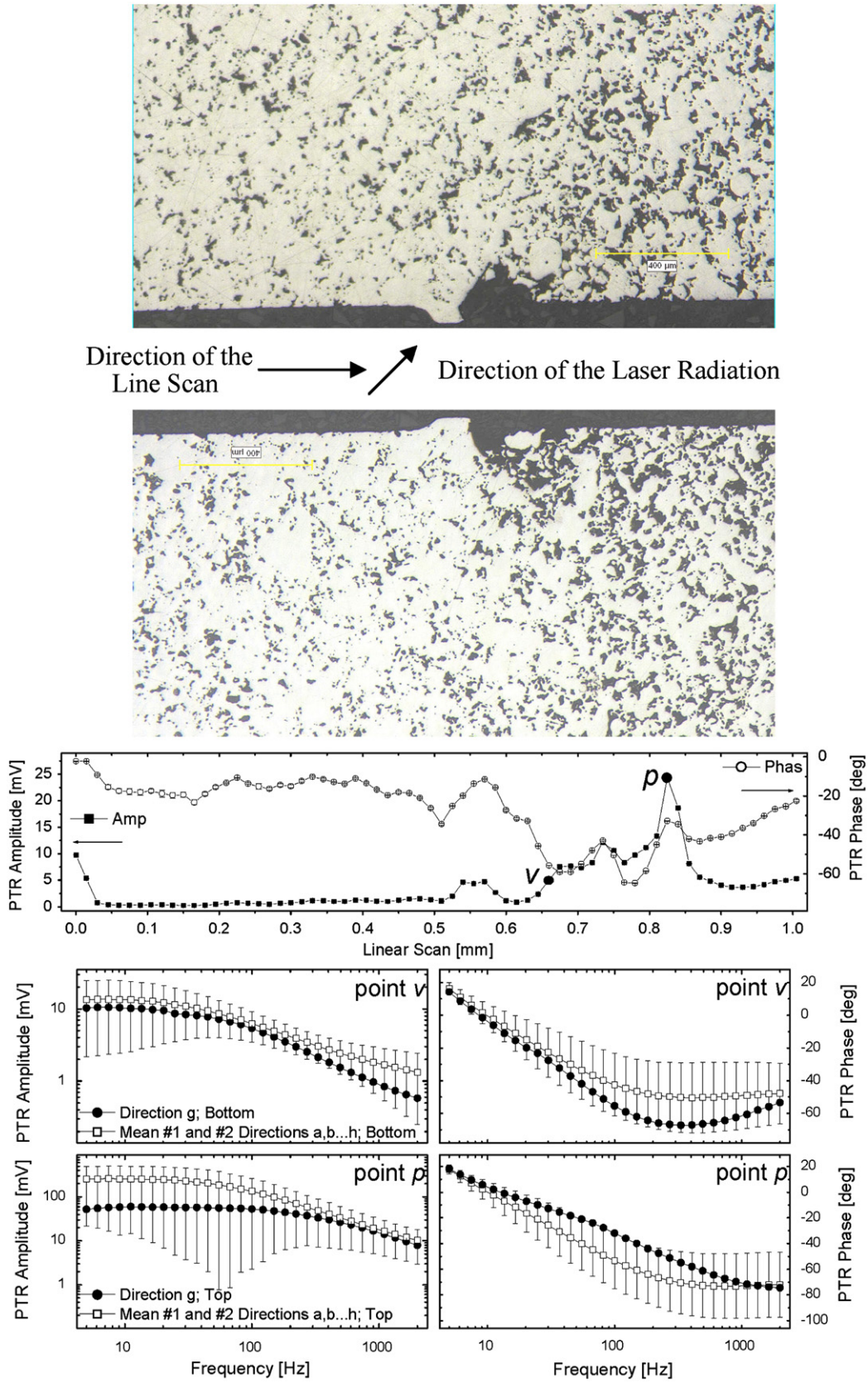


Fig. 6. Cross-sectional microscope pictures, radial line scan and frequency scans of green sprocket #1 at direction g.

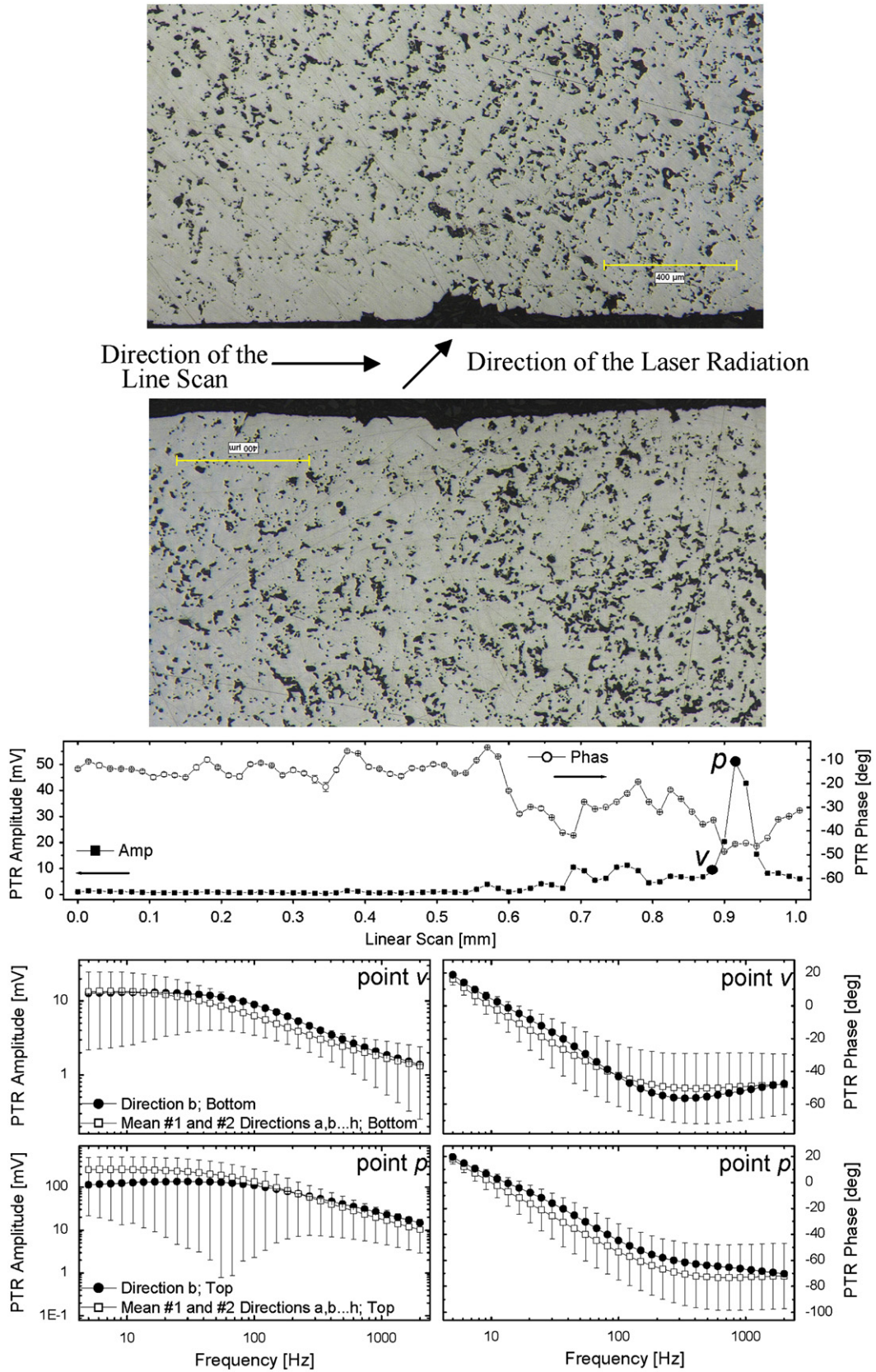


Fig. 7. Cross-sectional microscope pictures, radial line scan and frequency scans of green sprocket #2 at direction **b**.

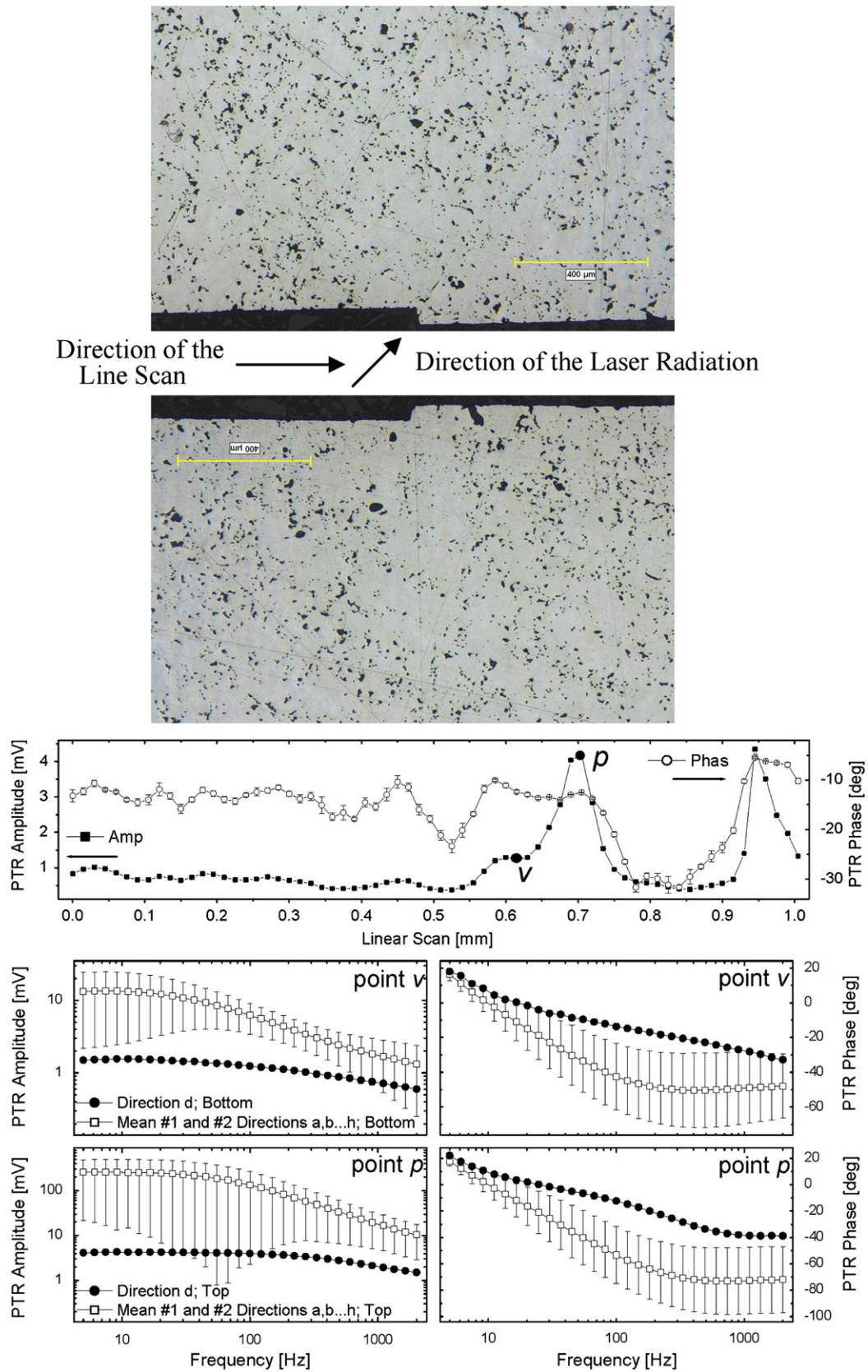


Fig. 8. Cross-sectional microscope pictures, radial line scan and frequency scans of green sprocket #3 at direction d.

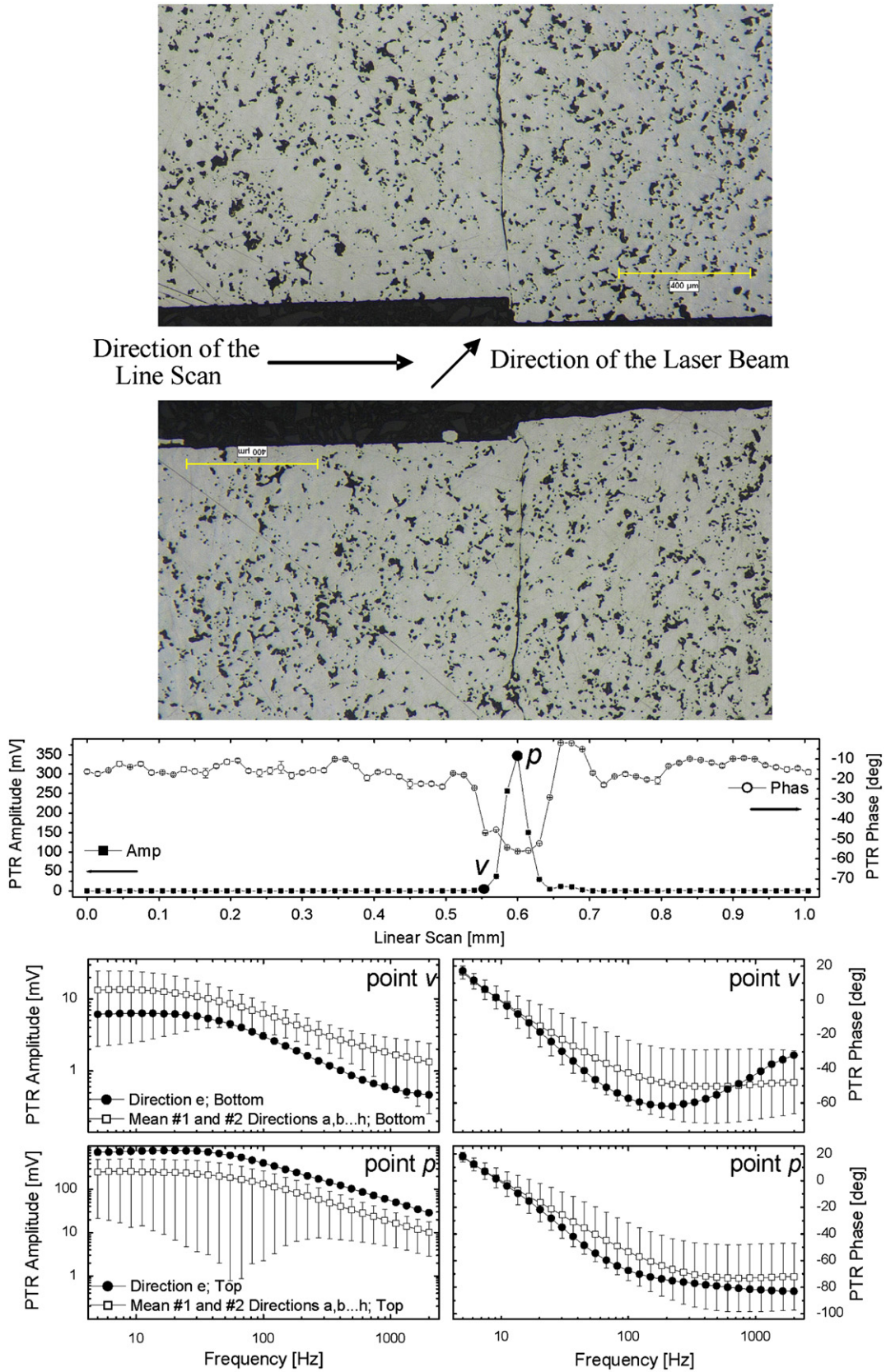


Fig. 9. Cross-sectional microscope pictures, radial line scan and frequency scans of green sprocket #4 at direction e.

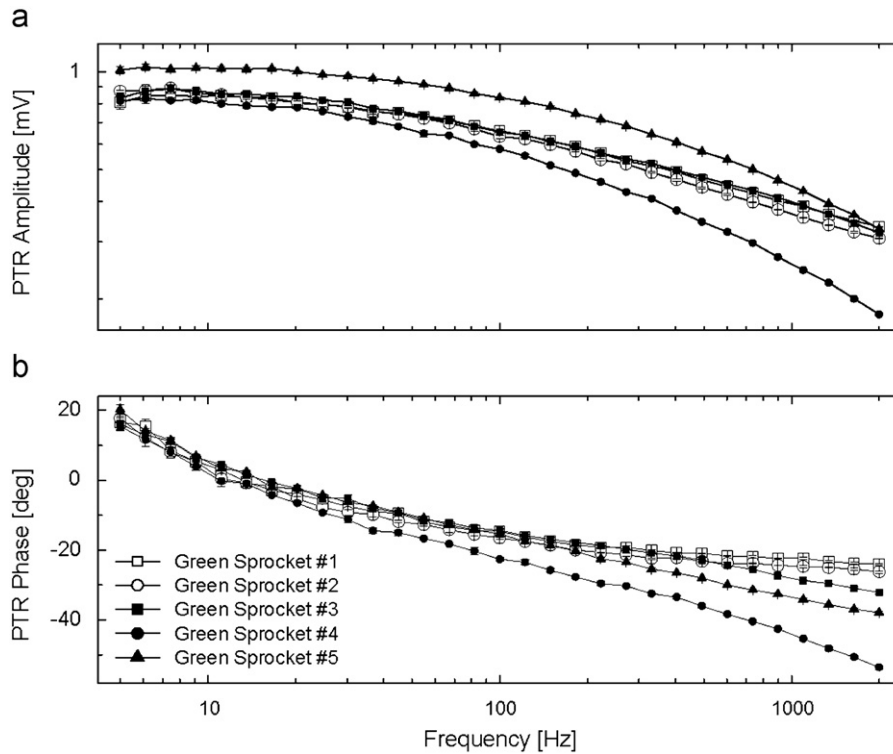


Fig. 10. Frequency scans of green sprocket samples at point TF, Fig. 2.

Table 1
Crack presence statistics for sprocket #3.

Point	Crack presence frequency scan phase signal	Crack presence pictures		Outcomes [prediction—actual value]
		Side 1	Side 2	
<i>Frequency scan signal phase</i>				
<i>Performed at the pedestal of radial line scan signal amplitude</i>				
A	Positive	Positive	Positive	True positive
B	Positive	Positive	Positive	True positive
C	Negative	Positive	Positive	False negative
D	Positive	Negative	Negative	False positive
E	Positive	Positive	Positive	True positive
F	Positive	Positive	Positive	True positive
G	Positive	Positive	Positive	True positive
H	Positive	Negative	Negative	False positive
Accuracy ^a =0.63				
<i>Frequency scan signal phase</i>				
<i>Performed at the peak of radial line scan signal amplitude</i>				
A	Positive	Positive	Positive	True positive
B	Positive	Positive	Positive	True positive
C	Negative	Positive	Positive	False negative
D	Positive	Negative	Negative	False positive
E	Positive	Positive	Positive	True positive
F	Positive	Positive	Positive	True positive
G	Positive	Positive	Positive	True positive
H	Positive	Negative	Negative	False positive
Accuracy ^a =0.63				

^a Accuracy=(TP+TN)/(TP+FN+TN+FN).

5. Discussion

The statistical analysis confirmed that over the entire set of sprockets investigated in this work, the sensitivity, specificity, and accuracy of the PTR crack detection technique are much better when probing the peak of the PTR signal at the inner step than when probing the foot of the signal distribution around the step.

This is likely so because cracks tend to form almost directly below the step, so the laser beam and the thermal wave are at the closest approach and most sensitive to subsurface cracks at that coordinate point. It was also mentioned that the actual position of “point *v*” may vary from sample to sample since there was no accurate way for fixing the coordinates of that point, unlike the peak amplitude “point *p*”. Our effort to use the digital camera and

Table 2Sensitivity, specificity, and accuracy of crack presence at 40 points on green sprockets for two inspection locations ν and p .

Inspection method	Sensitivity ^a	Specificity ^b	Accuracy ^c	Size of sample (points, n)
Frequency scan signal phase performed at the foot of radial line scan signal amplitude (point ν)	0.77 (17/22)	0.56 (10/18)	0.68	40
Frequency scan signal phase performed at the peak of radial line scan signal amplitude (point p)	0.91 (20/22)	0.61 (11/18)	0.78	40

P=true positive+false negative; N=true negative+false positive.

^a In parentheses: true positive/P.

^b In parentheses: true negative/N.

^c In parentheses: (true positive+true negative)/(P+N).

a semi-transparent mobile mirror to determine visually the inner step position was not effective because of the low-resolution image and impossibility of simultaneous PTR measurements and camera monitoring of the laser spot position on the sprocket surface in the present system design. In view of this inability, the locations of step and frequency-scan coordinates were defined by PTR signal line scans alone. Therefore, the level of roughness of the sample surface and variations in the spatial profile of the step (see variations in step-profiles of cracked and non-cracked sprockets in Figs. 4 and 5, and Figs. 6 and 7, respectively) influences the selection of the frequency scan coordinates and may have compromised the statistics of the PTR technique. Indeed, the statistical calculation shows that at peak point p the sensitivity of the technique is excellent: within the limited statistical sample of these measurements, there is 91% probability that a positive PTR reading is the result of a true crack. The specificity is not as good: there is 61% probability that a negative PTR reading is the result of the absence of a crack. We believe that the existence of many false positive results is related to local roughness irregularities in the neighborhood of the step. In our present setup, we cannot avoid these signal fluctuation factors because we have limited laser power and very small spot size (20 μm) of the focused laser beam, commensurate in size with interfering surface material clusters. The accuracy is significantly higher at 78%. We now discuss in some more detail the eight test measurements at peak point p in terms of the statistical results for each of the five sprockets:

1. *Sprocket #3*: Five instances of crack presence were confirmed, one location gave false negative information, and two locations gave false positive information (see Fig. 3, frequency scans, and Table 1). At 62.5% true crack positives, sprocket #3 would have been labeled “cracked” under non-destructive PTR interrogation alone. Indeed, the sprocket had been labeled “cracked” by the manufacturer before being subjected to PTR crack analysis.
2. *Sprocket #4*: Seven test results confirmed the presence of subsurface cracks along the various radial directions, with one test result giving a false negative. At 87.5% true crack positives, sprocket #4 would have been labeled “cracked” under non-destructive PTR interrogation alone. Indeed, the sprocket had been labeled “cracked” by the manufacturer.
3. *Sprocket #5*: All eight test results confirmed the presence of subsurface cracks along the various radial directions. At 100% true crack positives, sprocket #5 would have been labeled “cracked” under non-destructive PTR interrogation alone. Indeed, the sprocket had been labeled “cracked” by the manufacturer.
4. *Sprocket #1*: Six test results confirmed the absence of subsurface cracks while two test results gave false positive indications. At 75% true crack negatives, this sprocket would have been labeled crack-free under non-destructive PTR interrogation alone when the 61% specificity and 75% accuracy are taken into consideration. Indeed, the sprocket had been

labeled “crack-free” by the manufacturer before being subjected to PTR crack analysis.

5. *Sprocket #2*: Five test results confirmed the absence of subsurface cracks while three test results gave false positive indications. At 62.5% true crack negatives, this sprocket could have been labeled crack-free under non-destructive PTR interrogation alone, also when the 61% specificity and 63% accuracy are taken into consideration. Indeed, the sprocket had been labeled “crack-free” by the manufacturer.

In terms of the future possibility of this statistical crack inspection methodology to qualify for industrial production settings the measurement time (currently ca. 20 min per frequency scan) has to reduce to the range 20–50 s. To attain this level of speed one can use swept sine (ms duration, or approx. 1 s for 500–1000 co-added sweeps) and cross-correlation methods, as well as higher laser power to obtain stronger thermal-wave signals and to minimize the time of integration and number of measurements.

6. Conclusions

It has been shown that photothermal radiometry can be a valuable NDT technique for monitoring the presence of subsurface hairline cracks created during the forming process of green automotive parts. The use of modulated and focused laser beam as a precise heat-generating source allows the use of the extremely sensitive phase measuring lock-in technique that eliminates the influence of surface texture, roughness, and cleanliness. The small laser beam spot size allows forming a thermal wave within 1–2 thermal diffusion lengths in volume elements where the probability of crack appearance is high such as at steps and edges. This work is very promising for establishing a new in-line NDT methodology for subsurface crack detection in unsintered (green) automotive parts, in view of the fact that photothermal signals from these parts are quite strong, sensitive and specific to the cracks, and there is no other NDT method available for on-line monitoring of these manufacturing defects. The contrast of the mid-IR dc imaging technique [6–9] is limited by the accuracy of crack pattern recognition with respect to a reference image and by the absence of thermal diffusion length to optimize contrast. Furthermore, the thermal image generated by one pixel represents 0.5–1.0 mm characteristic length on the imaged surface. Therefore, a μm -size crack has only a minor influence on the detected thermal signal, which is integrated over the size of the pixel. Most importantly, the impact of powder clustering and surface irregularities, such as corners and steps, in PM automotive parts makes the background signal contributions very significant. The presented PTR technique overcomes this setback through frequency analysis of the photothermal signal generated in the presence of 20 μm (or thinner) cracks in the neighborhood of locations of high stress in our samples (corner or step).

A statistical analysis of the experimental PTR frequency scan phase data performed at sixteen points on the surface of five green

sprockets was presented. The lower specificity and accuracy of the PTR technique than its sensitivity may be explained by the variance in inner step shapes and angles of the manufactured sprockets tested in this work, the inability to effect adequate visual localization of the probed coordinate points, as well as by fluctuations in thermophysical properties of the green samples which are undoubtedly present within the particulate agglomerates that appear randomly distributed in the vicinity of the steps of the green samples.

Acknowledgements

We are thankful to the Ontario Centres of Excellence (OCE), and in particular to Materials and Manufacturing Ontario (MMO) and to Stackpole, Inc., for funding of this project.

References

- [1] Proceedings of the 2008 World Congress on Powder Metallurgy & Particulate Materials, June 8–12, Washington, DC.
- [2] Munidasa M, Mandelis A, Ferguson C. Resolution of photothermal tomographic imaging of subsurface defects in metals with ray optic reconstruction. *Appl Phys A* 1992;54:244–50.
- [3] Inglehart LJ, Grice KR, Favro LD, Kuo PQ, Thomas RL. Spatial resolution of thermal wave microscopes. *Appl Phys Lett* 1983;43(5):446–8.
- [4] Grice KR, Inglehart LJ, Favro LD, Kuo PQ, Thomas RL. Thermal wave imaging of closed cracks in opaque solids. *J Appl Phys* 1983;54(11):6245–55.
- [5] Munidasa M, Mandelis A. Photopyroelectric thermal-wave tomography of aluminum with ray-optic reconstruction. *J Opt Soc Am A* 1991;8(12):1851–8.
- [6] Benzerrouk S., Ludwig R. An infrared imaging approach for quality assurance in the powder-metallurgy process. In: Proceedings of the 2008 world congress on powder metallurgy & particulate materials, June 8–12, Washington, DC.
- [7] Benzerrouk S., Ludwig R., Apelian D. Electrothermal defect detection in powder metallurgy compacts. In: Proceeding of the 2005 international conference on the review of progress in quantitative nondestructive evaluation, vol. 25, American Institute of Physics. p. 1201–8.
- [8] Benzerrouk S, Ludwig R. Infrared detection of defects in powder-metallic compacts. *J Nondestruct Eval* 2007;26(1):1–9.
- [9] Benzerrouk S., Ludwig R., Apelian D. On-line testing of green-state compacts through active and passive thermography. In: International Conference on Powder Metallurgy and Particulate Materials, PowderMet07 Denver, CO, May 13–16, 2007.
- [10] O'Brien R.C., James W.B. Nondestructive inspection of powder metallurgy parts. *ASM handbook volume 17, nondestructive evaluation and quality control*. 1989. p. 536–48.